(This is a sample cover image for this issue. The actual cover is not yet available at this time.)

Earth and Planetary Science Letters 357–358 (2012) 68–77

Contents lists available at SciVerse ScienceDirect

Earth and Planetary Science Letters

journal homepage: www.elsevier.com/locate/epsl

Cluster analysis of global lower mantle tomography: A new class of structure and implications for chemical heterogeneity

Vedran Lekic [a,b,*], Sanne Cottaar [c], Adam Dziewonski [d], Barbara Romanowicz [c,e,f]

[a] Department of Geology, University of Maryland, College Park, MD, USA
[b] Geological Sciences, Brown University, Providence, RI, USA
[c] Berkeley Seismological Laboratory, University of California, Berkeley, CA, USA
[d] Department of Earth and Planetary Sciences, Harvard University, Cambridge, MA, USA
[e] Collège de France, Paris, France
[f] Institut de Physique du Globe, Paris, France

ARTICLE INFO

Article history:
Received 2 June 2012
Received in revised form
8 September 2012
Accepted 14 September 2012
Editor: P. Shearer

Keywords:
seismic tomography
Earth's deep interior
mantle structure
D″
cluster analysis

ABSTRACT

Earth's lower mantle is dominated by a pair of antipodal large low shear velocity provinces (LLSVPs) that reach >1000 km up from the core–mantle boundary (CMB). These are separated by a ring of faster-than-average velocities thought to be related to subduction of oceanic lithosphere. How robustly does global tomography constrain velocity structure in the lower mantle, and are there other robust large scale features that have not been identified? We use cluster analysis to identify structures and seismic characteristics common to a set of recent global tomographic models which have been derived using different data sets, parameterizations, and theory behind approximations used in inversion. We detect a pronounced asymmetry in the velocity gradient with depth between seismically fast and slow regions in the lowermost 500 km of the mantle, suggesting the presence of compositional heterogeneity. We find that, in all models, there is a clear separation of lower mantle structure into one fast and two slow regions, and that the boundary of the regions is remarkably similar across models even on length scales as small as <1000 km. This inter-model similarity indicates that long wavelength features are not a consequence of lack of fine-scale resolution, but that they truly dominate the structure in the lowermost mantle. There is a single exception to this separation: an isolated slow anomaly ~900 km across (at the CMB) and extending ~500 km upward from the core–mantle boundary, which we call the "Perm Anomaly". Though it is far smaller than an LLSVP, waveform analysis confirms that this anomaly is robustly constrained and bounded by rapid lateral velocity gradients like those found around LLSVPs, suggesting that the nature and process of formation of both types of structures may be related.

1. Introduction

The fact that the bottom 1000 km of the mantle is dominated by very large scale velocity anomalies is well established; spherical harmonic degrees two and three contain 70% of the power in a set of recent shear wavespeed (Vs) tomographic models (Dziewonski et al., 2010). The two prevailing features are called African and Pacific Superplumes (also, Large Low Shear Velocity Provinces, Garnero and McNamara, 2008, LLSVPs) and their shape is well represented by spherical harmonic degrees two and three (Dziewonski et al., 2010). In Fig. 1a–e, maps of lateral variations of Vs at a depth of 2800 km for five recent tomographic models (SAW24B16: Mégnin and Romanowicz, 2000; HMSL-S: Houser et al., 2008; S362ANI: Kustowski et al., 2008; GyPSuM: Simmons et al., 2010; S40RTS: Ritsema et al., 2011) show that the African and Pacific LLSVPs are surrounded by a ring of faster-than-average shear velocities. This pattern is even apparent in the measurements of travel times of shear waves that are sensitive to lower mantle structure (Fig. 1f; Manners, 2008). Are there other robust, large-scale features that have not been identified? We describe here an experiment designed to answer this question, in which cluster analysis is used to identify common features of and differences among these five lower mantle Vs models.

The tomographic models we analyze were derived using different datasets, parameterization, regularization, and theory behind approximations used in inversion (see Table 1). Multiple studies have demonstrated that differences in parameterization (Trampert and Snieder, 1996; Boschi and Dziewonski, 1999; Spetzler and Trampert, 2003), regularization (Trampert and Spetzler, 2006), and theoretical

* Corresponding author at: Department of Geology, University of Maryland, College Park, MD, USA. Tel.: +1 301 405 4086.
E-mail address: ved@umd.edu (V. Lekic).

0012-821X/$ - see front matter © 2012 Elsevier B.V. All rights reserved.
http://dx.doi.org/10.1016/j.epsl.2012.09.014

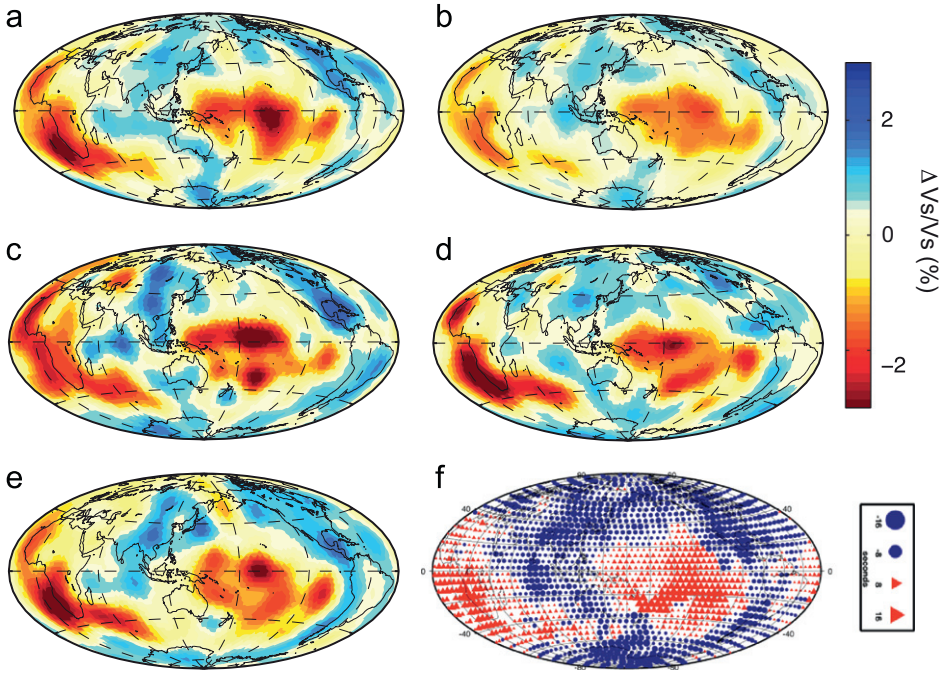

Fig. 1. (a–e) Maps of lateral Vs variations at 2800 km depth in the 5 tomographic models analyzed in this study (a: Kustowski et al., 2008; b: Ritsema et al., 2011; c: Mégnin and Romanowicz, 2000; d: Houser et al., 2008; e: Simmons et al., 2010). All the models are filtered to include power up to spherical harmonic degree 18. The maps are split at 30°W. Note the dominance of the degree-2 structure – antipodal large low shear velocity provinces ringed by faster-than average regions – as well as the slow anomaly beneath western Siberia. (f) Both of these features are apparent in the measurements of travel-times of shear waves that are sensitive to lower mantle structure (Manners, 2008), here binned in 5° caps and plotted at the turning (S) or bounce points (ScS) or midpoints of the path along core-mantle boundary (Sdiff). Note that norm damping used in the construction of S40RTS partially accounts for the smaller amplitude of lateral variations of Vs in that model (b). (a) S362ANI, (b) S40RTS, (c) Saw24B16, (d) HMSL-S, (e) GyPSuM and (f) S, Sdiff,ScS-S residuals.

Table 1
Parameterizations, datasets, theoretical frameworks, and regularization schemes used in the construction of the global Vs models analyzed in this study.

Tomographic model	Parameterization		Lower mantle data	Theoretical Framework	Regularization
	Horizontal	Vertical			
SAW24B16	Spherical harmonics up to degree 24	16 cubic b-splines	Transverse component waveforms ($T>30$ s) subdivided into wave packets to isolate body waves from fundamental mode surface waves	Full waveform inversion via non-linear asymptotic coupling theory NACT (Li and Romanowicz, 1995)	A priori model covariance matrix incorporating norm damping, horizontal and vertical first-derivative and vertical second derivative smoothing
HMSL-S	4° blocks	18 layers of equal thickness	S, SS travel-times from transverse component cross-correlation ($T>15$ s), hand-picked SS-S and ScS-S differential measurements	Ray theory with 1D ray tracing	Horizontal and vertical smoothing
GYPSUM	275 km × 275 km blocks	22 layers (75–240 km thick)	S, sS, ScS, sScS, SKS, SKKS travel times ($T>14$ s), P summary travel times, horizontal plate divergence model, free-air gravity model, dynamic topography model, excess ellipticity of core–mantle boundary	Ray theory with 1D ray tracing, viscous flow in a radially symmetric viscosity profile	Second derivative horizontal and vertical smoothing
S40RTS	Spherical harmonics up to degree 40	21 vertical splines, spacing increasing with depth	Normal mode splitting ($T>333$ s) functions, cross-correlation travel-times of S, Sdiff, SS, SSS and major-arc SS_M, SSS_M, $SSSS_M$, and SKS, SKKS on radial component	Ray theory with 1D ray tracing, normal mode splitting related to Vs through depth-dependent kernel functions computed in PREM (Dziewonski and Anderson, 1981)	Norm damping
S362ANI	362 spherical splines	16 cubic splines, discontinuous across 650 km	Long period waveforms of body ($T>50$ s) and mantle ($T>125$ s) waves. Travel times of S, SS, ScS, ScSScS, SS-S, ScS-S, S-SKS, SKKS-SKS, SS-S, ScS-S obtained using cross-correlation, with dominant period of 20 s	Full waveform inversion of body ($T>50$ s) and mantle waves ($T>125$ s) via path-average approximation PAVA (Woodhouse and Dziewonski, 1984); ray theory with 1D ray tracing for travel time data	Horizontal and vertical smoothing

approximations (Megnin and Romanowicz, 1999; Clevede et al., 2000; Montelli et al., 2004) can lead to substantial differences in the resulting tomographic models, especially in locations where data constraints are few or ambiguous. Velocity structures common across tomographic models are, therefore, likely to be robustly constrained by multiple sets of available seismic data. In other words, while

particular features of a single tomographic model may reside in the null space and be the result of a particular choice of model parameterization, regularization or theoretical approximation, this is unlikely for features common across tomographic models.

2. Method

Cluster analysis is an objective way of assigning organisms, objects, or observations into groups whose members are relatively homogeneous or similar to one another compared to the population at large. Cluster analysis can be described as objective in the sense that similarity or difference between members is quantified through a distance metric; on the other hand, the choice of the distance metric and the definition of distance between groups of individuals can be chosen to suit the particular application or highlight a particular feature. Because it is easily replicable and capable of tackling high-dimensional data gathered by a variety of methods, cluster analysis has found widespread use: marketing (e.g. Punj and Stewart, 1983), sociology (e.g. Filsinger et al., 1979), psychology (e.g. Evritt et al., 1971), ecology (e.g. Beibin and McDonald, 1993), hydrology (e.g. Harris et al., 2000), volcanology (e.g. Luhr et al., 2010), seismology (e.g. Houser et al., 2008).

When applied to profiles of shear wavespeed (Vs) variations beneath different locations on Earth, cluster analysis can group Vs profiles according to their similarity to one another. Because the quantitative measure of similarity is specified through a distance metric and is applied to all profiles, the classification of Vs profiles through cluster analysis is automatic and reproducible. Furthermore, as each Vs profile corresponds to a location on the Earth's surface, each group/cluster of similar Vs profiles corresponds to a set of points on the surface of the Earth, tracing out geographic regions in which the depth variation of Vs is similar. Lekic and Romanowicz, 2011 found that for the upper mantle, the geographic regions of clusters of similar Vs profiles correspond to the signature of surface tectonics; this was the case for both Euclidean and correlation distance metrics. Furthermore, they showed that the comparison of geographic extents of individual clusters enabled straightforward assessment of similarities and differences between tomographic models.

Here, we apply cluster analysis to the lower mantle in order to identify characteristics that are present in all of the global Vs tomographic models. We extract profiles of absolute shear wave speed from each of the five tomographic models – SAW24B16, HMSL-S, S362ANI, GyPSuM, S40RTS – beneath a set of 2562 equally-spaced (average spacing is $\sim 4^{\circ}$) points on the Earth (Wang and Dahlen, 1995) in the 1000–2800 km depth range (sampled every 50 km resulting in sampling at 37 individual depths). Because of differences in horizontal parameterizations and because very little power is contained in higher spherical harmonic degrees, we filter the models to exclude power at spherical harmonic degrees >12. The very bottom of the tomographic models (at depths exceeding 2800 km) is not included in our analysis since the structure in this depth range may be affected by artifacts associated with the edge of the model space at the CMB.

For each model, the Vs profiles are treated separately, resulting in 2562 vectors residing in 37-dimensional space; each vector corresponds to a location on the surface of the Earth, and its coordinates specify the Vs at depth. We define distance between individual Vs profiles as the squared Euclidean distance between these vectors. It is worth noting that this choice of distance measure will make the cluster analysis more dependent on regions where the amplitude of Vs variations is large; in our case, this is the bottom 500 km of the mantle. The Vs profiles are then grouped into k families using k-means clustering (MacQueen, 1967), where k is a pre-assigned integer. Since each point on the Earth can then be associated with one of the families, k geographic regions are traced out.

k-means is an efficient way of partitioning a large set of objects (such as the 37-dimensional vectors that represent the profile of Vs beneath each point) into k clusters (groups) so that the within-cluster variance is small. Each cluster is associated with an average vector (Vs profile) for that cluster, and each Vs profile is associated with one and only one cluster. The k-means procedure is initialized by k randomly selected Vs profiles, which serve as the starting point for clustering of a decimated set of Vs profiles. The mean Vs profiles of the clusters that result from this initial clustering then seed the k-means procedure that is performed on the complete set of Vs profiles. We repeat this entire procedure 5 times in order to help ensure that the k-means procedure converges to the set of clusters that minimize the intra-cluster variance. We use the MATLAB implementation of the k-means algorithm.

In contrast to the upper mantle, where increasing k from 2 to 6 progressively brings out significant new tectonic features (Lekic and Romanowicz, 2011), we find that, for the lower mantle, $k=2$ is sufficient to capture the first order structural units (i.e. the LLSVPs), characterized respectively by uniformly slower or faster Vs compared to the reference 1D model (PREM: Dziewonski and Anderson, 1981). For each cluster, we construct a single representative velocity profile by averaging the constituent Vs profiles within that cluster. We also construct a map that associates with each location on the Earth an integer ranging from 0 to 5; this integer represents a count of how many tomographic models assigned that particular point to the slow cluster, a sort of "voting" scheme to assess the robustness of the clustering with respect to individual models.

3. Results

3.1. Consistency of tomographic models

This "vote" map (Fig. 2) shows that the geographic extents of the two clusters of Vs profiles trace out a fairly simple pattern in all five tomographic models, dividing the globe into two slow and one fast region. This geographic contiguity is not a peculiarity of

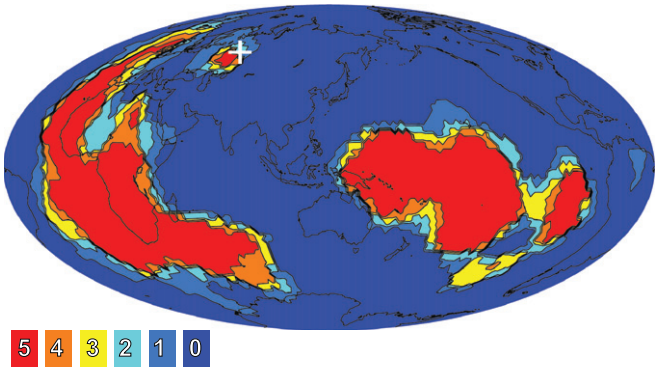

Fig. 2. Cluster analysis of shear velocity (Vs) profiles (1000–2800 km depth range) from five recent global tomographic models (Mégnin and Romanowicz, 2000; Houser et al., 2008; Kustowski et al., 2008; Simmons et al., 2010; Ritsema et al., 2011) in the lower mantle defines two regions whose geographic extents are consistent across models, tracing out the African and Pacific LLSVPs, as well as a single, globally-contiguous faster-than-average region. Pixels that make up this map are color-coded according to how many models assign the Vs profile beneath that point to the slow cluster, and the map is split at 50°W. The models are spatially filtered to exclude power at spherical harmonic degrees >12. Reconstructed location (Torsvik et al., 2008) of the center of Siberian Trap eruptions is indicated by the white cross. (For interpretation of the references to color in this figure legend, the reader is referred to the web version of this article.)

the cluster analysis technique, which is unaware of the geographic locations of the model vectors of velocities. Instead, it is a defining and surprising characteristic of the lower mantle which is partly the result of the dominance of longest-wavelength structure within the lower mantle in general, and within its lowermost 500 km in particular, where the larger amplitudes of Vs anomalies have a greater influence on the results of the cluster analysis. Shorter-wavelength structure exhibits itself primarily through undulations of the LLSVP boundaries.

The great preponderance of 0 and 5 counts, as compared to intermediate values, indicates a high level of consistency among tomographic models in assigning a given Vs profile (and its associated geographic location) to a particular cluster. Should this high level of inter-model consistency be interpreted to imply that all the models are successfully resolving true lower mantle structure, or that all the models simply share common inadequacies? We prefer the former interpretation for two reasons: (1) shear waves sample the lower mantle well and offer complete global coverage (see Fig. 1f); (2) model parameters that are less-well constrained by available data would tend to exhibit greater inter-model variability, since the differences in parameterization, regularization, and theoretical approximations (see Table 1) would be more consequential in these regions. Therefore, while areas characterized by intermediate vote counts may well represent poorly-resolved regions, the preponderance of 0 and 5 counts indicates that the large-scale features of lowermost mantle structure are presently well known.

The two main regions associated with the slower cluster are the LLSVPs. The African one is elongated in the North–South direction with a very sharp transition from 0 to 5 counts on the western and eastern sides, signifying that this boundary is found in the same location in all 5 tomographic models. The only region within the African LLSVP that exhibits substantial inter-model diversity is found beneath central Africa; this diversity may reflect either structural complexity, or less robust data constraints. With one exception, the boundaries of the Pacific LLSVP are also collocated across all five tomographic models. However, its eastern part may be "detached" from the main body, although three of the five models suggest continuity. Nevertheless, the cluster's geographic extent narrows substantially, reflecting a perturbation in the shape of this otherwise fairly-uniformly slow region. All tomographic models agree that the geographic extent of the faster cluster is globally contiguous.

Detailed studies of waveforms of shear waves (Sdiff, ScS, and/or SKS) sampling along the margins of the LLSVPs have demonstrated that strong lateral gradients in velocity bound the African plume to the west/southwest (Wen et al., 2001; Ritsema et al., 1998) and southeast (Ni, Helmberger and Tromp, 2005; Ni et al., 2002a, b; Wen, 2001a, b; To et al., 2005). Similarly sharp boundaries have been observed across the northwestern/western (He et al., 2006; Takeuchi et al., 2008), southwestern (He and Wen, 2009), southeastern (To et al., 2005), and northern (Cottaar and Romanowicz, in press) boundaries of the Pacific LLSVP. We find that the locations of LLSVP boundaries detected in these studies are remarkably consistent with the boundaries traced out by our cluster analysis of global tomographic models. This agreement appears to extend to small scales: the <1000 km-wide divot in the Pacific LLSVP present in the vote map (Fig. 2) in the vicinity of Tonga may well give rise to the LLSVP "gap" detected using SKS travel times by He and Wen (2009).

How do the geographic extents of the slow and fast clusters vary with depth, from mid-mantle to the lowermost mantle? We perform cluster analysis on Vs profiles extracted in the 800–1800 km and 1800–2800 km depth ranges and compare the results to those obtained for the entire lower mantle (left column of Fig. 3). We find that the geographic extents of slow and fast clusters for the whole mantle (see Fig. 2) reflect structure in the 1800–2800 km range (bottom Fig. 3), where lateral variations of Vs are greatest. In the mid-mantle (top, Fig. 3), inter-model

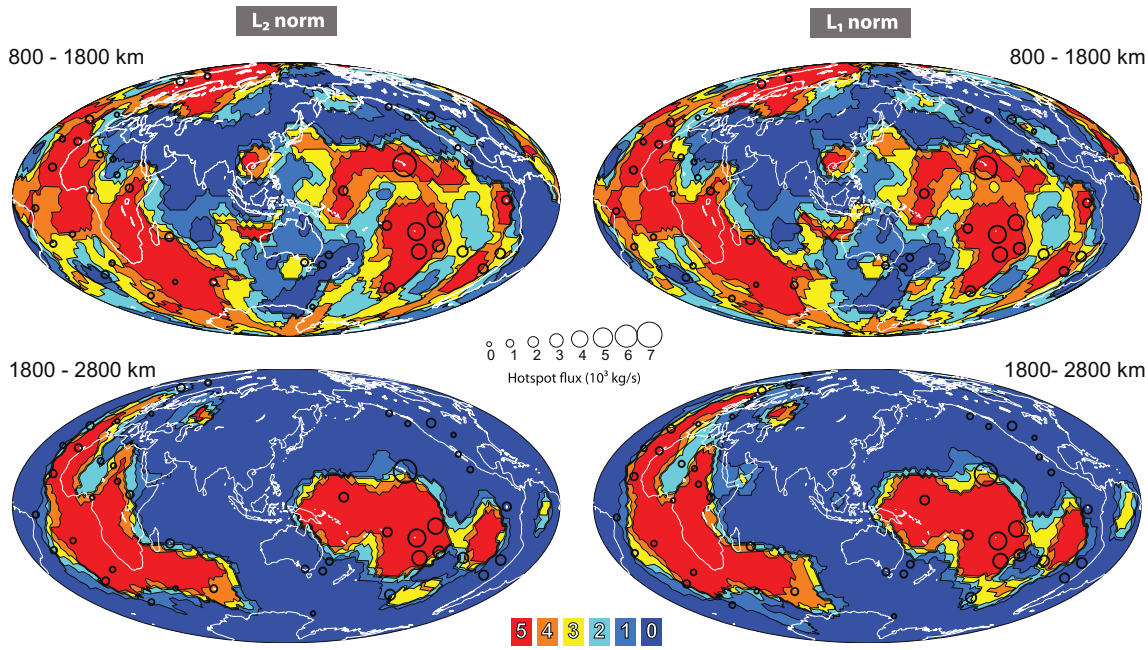

Fig. 3. The effect of distance metric and choice of depth range of Vs profiles on geographic extents of the slow and fast clusters. As in Fig. 2, pixels that make up this map are color-coded according to how many models assign the Vs profile beneath that point to the slow cluster, and all 5 tomographic models are filtered to exclude power at spherical harmonic degrees >12. The choice of squared Euclidean distance ($L2$ norm) vs. "city-block" distance ($L1$ norm) has only minor effect on the retrieved geographic extents of clusters. However, the geographic extent of clusters of Vs profiles for the upper lower mantle (800–1800 km) differs from that for the lowermost mantle (1800–2800 km) in that the slow cluster becomes more geographically distributed and inter-model variability increases. Locations of surface hotspots are denoted by black circles, whose size is proportional to their inferred anomalous mass flux (Steinberger, 2000). The geographic extents of slow and fast clusters for the whole mantle (Fig. 2) reflect structure in the 1800–2800 km range, where lateral variations of Vs are greatest, regardless of whether the L1 or L2 distance metrics are used. (For interpretation of the references to color in this figure legend, the reader is referred to the web version of this article.)

variability increases somewhat, though the general distribution of slow and fast regions is similar to that in the lowermost mantle, consistent with the strong vertical continuity of seismically slow regions identified in radial correlation functions throughout the lower mantle (Dziewonski,et al., 2010; Jordan et al., 1993). The region assigned to the slow cluster becomes more geographically fragmented in the mid-mantle. Beneath the Pacific, it comprises three main pieces that three out of five tomographic models find to be interconnected: one arching from Hawai'i toward the Caroline hotspot, another extending from Louisville to Society/Marquesas/MacDonald/Pitcairn hotspots, and another stretching from Galapagos down to Juan Fernandez. Beneath Africa/Atlantic, the slow region remains more continuous, stretching from Kerguelen, past Reunion and Afar all the way to Iceland. We verify that the particular choice of squared Euclidean distance (L_2 norm) vs. "city-block" distance (L_1 norm) has a very minor effect on the retrieved geographic extents of clusters in both the mid and lowermost mantle (Fig. 3).

We can also look at both inter-model consistency and vertical continuity of structure in the wavenumber domain. In Fig. 4, we compare the spherical harmonic coefficients of the 5 tomographic models as a function of spherical harmonic degree and depth. We find that the inter-model agreement and vertical consistency of low degree spherical harmonics coefficients is remarkably strong throughout the lowermost 1000 km, but weakens somewhat in the mid-mantle where the dominance of low degree (long wavelength) structure wanes and the spectrum of heterogeneity whitens. These wavenumber characteristics of tomographic models reflect the changes in geographic extents of the slow and fast clusters at mid-mantle depths (Fig. 3). Specifically, the change in the spectrum from the deep to the mid-mantle reflects the broadening and breaking up of the low velocity region into somewhat smaller scale features; therefore, the waning of the degree 2 and 3 signal in the mid-mantle is not inconsistent with vertical continuity of slower-than-average structures throughout the lower mantle.

3.2. Asymmetry in lower mantle Vs profiles

Average Vs profiles of the two clusters are shown with respect to PREM (Dziewonski and Anderson, 1981) in Fig. 5 and demonstrate that there is good inter-model agreement and substantial asymmetry in behavior between the slow and fast clusters, reflecting the bimodal character of lower mantle velocity distributions (e.g. Hernlund and Houser, 2008). Velocities within the fast cluster have a similar gradient with depth as PREM, so that at nearly-all depths Vs deviates by less than 0.5% from the reference 1D model PREM. The velocity gradients with depth of the slow cluster, on the other hand, decrease markedly starting at ~2200–2400 km depth, resulting in Vs anomalies $>1\%$ w.r.t PREM for nearly all models at the base of the mantle. The bottom 500 km of the lower mantle, then, emerges as an anomalous region characterized by: (1) increased amplitude of lateral Vs variations; (2) asymmetry of both the amplitude and vertical gradients of Vs between slow and fast regions.

We call this the "abyssal region" (not to be confused with the "hot abyssal layer" (Kellogg et al,. 1999), which term describes a compositionally distinct layer within the lower mantle) to distinguish it from the D″ region, which is defined by a change in the gradient of

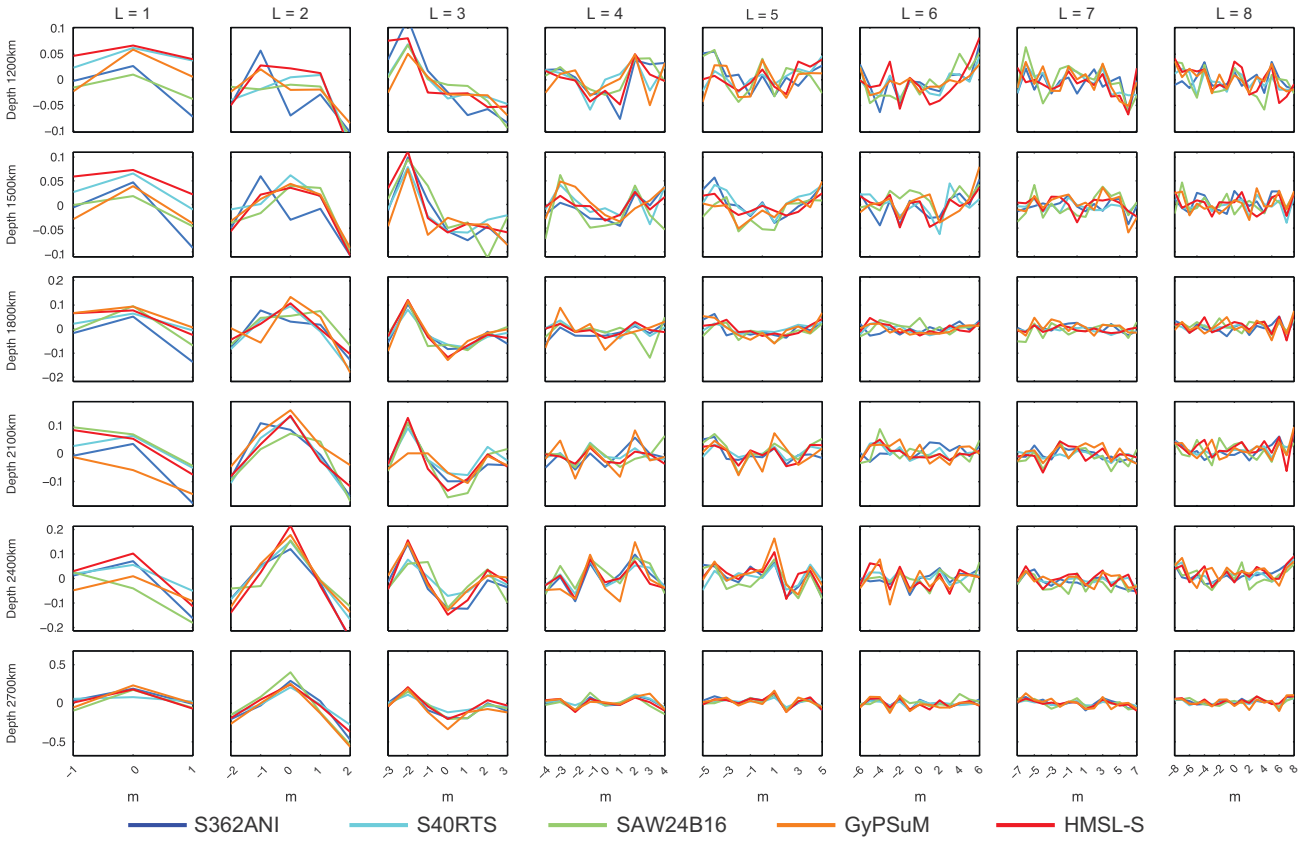

Fig. 4. Spherical harmonic coefficients for degrees 1–8 of the five tomographic models are shown between 1200 and 2700 km depth. Though there is a clear "whitening" of the spectrum going from deep to mid-mantle depths, degrees 1, 2, 3 remain robust throughout. The characteristic pattern of coefficients for these three degrees – which persists clearly in the lowermost 1200 km – is diagnostic of the familiar pattern of antipodal LLSVPs surrounded by a ring of faster-than-average velocities. The enhancement of degree 3 and higher signal in the mid-mantle reflects the broadening of the slow region visible in Fig. 3 in this depth range.

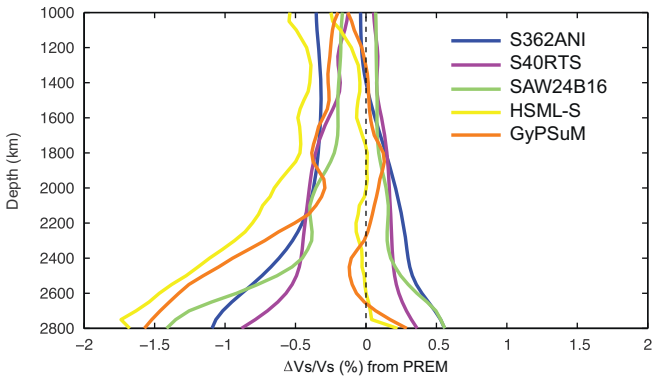

Fig. 5. Profiles of deviations of Vs with respect to PREM (Dziewonski and Anderson, 1981) in the fast and slow regions of five tomographic models (HMSL-S was constructed with respect to ak135 (Kennett et al., 1995) but refer PREM in this figure). In the bottom 500 km of the mantle ("abyssal region"), slow clusters are characterized by stronger Vs anomalies than the fast clusters. Equivalently, the velocity gradient with depth is substantially smaller in the slow cluster than in the fast cluster, where the gradient of velocity with depth is similar to that in PREM throughout the lower mantle.

the global average seismic velocity profile. It is likely that the abyssal and D″ regions are related in some fashion, though the abyssal region as seen by tomography appears to have a greater vertical extent; whether it is thinner in reality than it appears in the tomographic images is an open question, beyond the resolution afforded by current tomography. The fact that Vs of the slower cluster remains slower than average well above the abyssal region is consistent with cluster analysis of mid-mantle structure (see Fig. 3) and the coherence of degree 2 and 3 structure throughout the lower mantle (Fig. 4). This vertical continuity of slow Vs regions supports the argument that LLSVP regions are anomalously slow – and presumably have higher-than-average temperatures – even in the transition zone (Romanowicz and Gung, 2002).

The different gradients and amplitudes of Vs anomaly within the slow and fast cluster are consistent with a compositional component to the difference between the two regions. Compositional differences have been invoked to explain the sharp horizontal Vs gradients bounding the LLSVPs (Wen, 2001a, b; Ni et al., 2002a, b; To et al., 2005), the anticorrelation between bulk sound and shear wavespeeds (Su and Dziewonski, 1997; Robertson and Woodhouse, 1996; Masters et al., 2000), as well as the results of probabilistic tomography from normal mode splitting measurements used alone (Trampert et al., 2004) and along with body wave travel times and Rayleigh wave phase velocities (Mosca et al., 2012). Large temperature anomalies associated with the thermal boundary layer above the core–mantle boundary can produce large differences in the seismic attenuation between the slow and fast regions. However, attenuation cannot produce the anticorrelation between bulk sound and shear wavespeeds (Matas and Bukowinski, 2007) nor is it a straightforward explanation for the sharp lateral Vs gradients bounding the LLSVPs.

The presence of post-perovskite phase of $MgSiO_3$ (Murakami et al., 2004) in the seismically fast regions near the core–mantle boundary region has been invoked as an alternate explanation for these characteristics of Vs structure (Wookey et al., 2005), since ab initio calculations find that the perovskite (Pv) to postperovskite (pPv) phase transition is accompanied by an increase in Vs and a decrease in bulk sound speed (Oganov and Ono, 2004; Tsuchiya et al., 2004; Iitaka et al., 2004). In this view, the anticorrelation of Vs and bulk sound speeds and sharp lateral gradients in velocity can both be explained if Pv is preferentially present within slow regions (LLSVPs) and pPv in the fast regions. This model predicts that it is the Vs profile of the fast regions that should exhibit a change in velocity gradient with depth accompanying the Pv to pPv transition. This prediction should be tested against the asymmetric behavior of Vs profiles of slow and fast clusters in the abyssal region, specifically the marked deviation of the slow cluster's Vs profile from the global average.

Explaining the asymmetry between Vs profiles of fast and slow regions solely by the presence of pPv requires this phase to be stable >500 km up from the core–mantle boundary. Several laboratory studies have sought to constrain the stability field of pPv in a pyrolite composition: while some find that pPv might be stable in the required depth range at a temperature of 1500 K (Ohta et al., 2008), others find that the two phases are likely to co-exist throughout the bottom 300 km of the mantle depths (Andrault et al., 2010), or even that pPv may not actually be stable anywhere in the mantle even at these low temperatures due to the effects of Aluminum on the phase stability field (Grocholski et al., 2012). If the composition of the fast regions is closer to that of MORB, then the stability field extends to shallower depths, though it remains unclear whether the presence of pPv 500 km up from the core–mantle boundary is likely at realistic mantle temperatures.

3.3. A new type of lower mantle structure

By taking a closer look at the geographic extents of the two lower mantle clusters (Fig. 2) we see that there is a single exception to the simple division into one fast and two slow regions: there is a spatially small anomaly centered approximately beneath the city of Perm, Russia. Hence we call it the "Perm Anomaly", with no implied links to geological ages. This anomaly is resolved by all five models. Though somewhat model-dependent, its diameter is <1000 km (at the CMB) or $<1/25$th of the area of either LLSVP, and it appears to be well separated from the northern part of the African LLSVP. This separation is apparent in the raw seismic travel time data; a band of faster-than-average velocities separates the Perm Anomaly from the northern part of the African LLSVP in the S, ScS-S, and Sdiff residuals shown in Fig. 1f. Shear wavespeeds found within the Perm Anomaly (Fig. 6) are slower than the global average in the bottom 500 km in all five tomographic models; this makes the Perm Anomaly substantially shorter in height than an LLSVP, at least within the resolution of the present study. Nevertheless, it is an order of magnitude taller than ultra-low velocity zones (ULVZs) that are

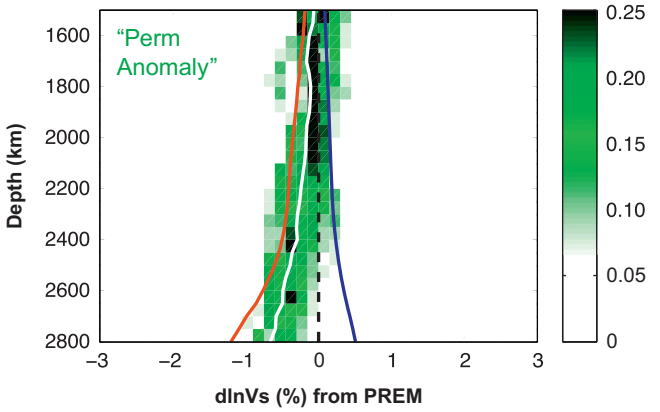

Fig. 6. Color density plots of Vs anomalies as a function of depth in the five tomographic models show that the "Perm Anomaly" (white profile) is significantly slow with respect to PREM in the bottom ~500 km of the lower mantle. Green shading is proportional to the fraction of Perm Anomaly Vs profiles within each ΔVs/Vs and depth bin. Average profiles of the fast (blue) and slow (red) clusters across all models are shown for reference. (For interpretation of the references to color in this figure legend, the reader is referred to the web version of this article.)

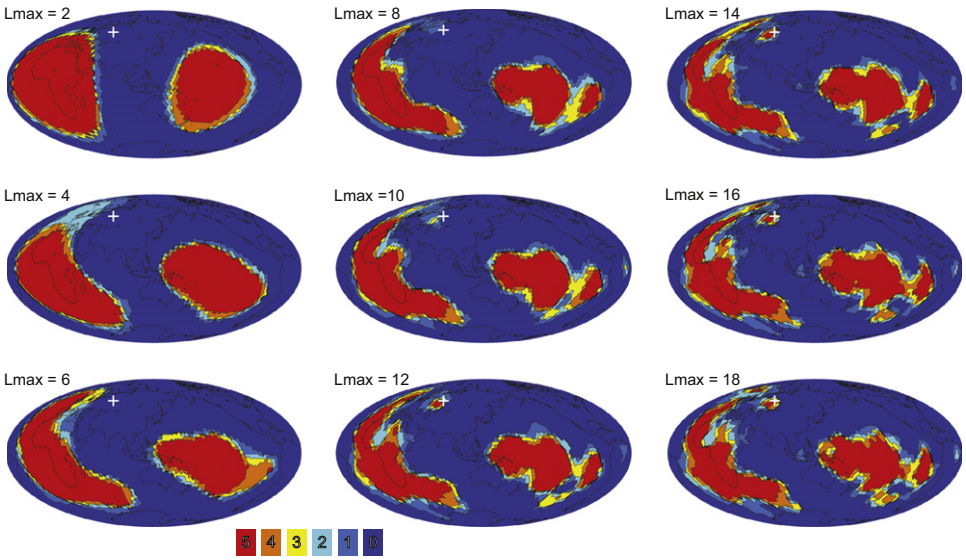

Fig. 7. Maps of the geographic extents of the fast and slow clusters for the five tomographic models analyzed (see Fig. 2). The pixels that make up this map are color-coded according to how many models assign the Vs profile beneath that point to the slow cluster. The models are spatially filtered to exclude power at spherical harmonic degrees $>L_{max}$, so that progressively smaller-scale features are included as L_{max} increases. Note that the emergence of the Perm Anomaly for all 5 models starting at $L_{max}=12$, and the remarkable agreement in the shape of the LLSVPs across tomographic models and across the range of L_{max}. (For interpretation of the references to color in this figure legend, the reader is referred to the web version of this article.)

often found in the vicinity of LLSVP margins (Thorne and Garnero, 2004; McNamara et al., 2010).

The vote map shown in Fig. 2 was obtained using versions of the five tomographic models expanded in spherical harmonics up to degree $L_{max}=12$. In Fig. 7, we compare voting maps obtained with the same five models, but successively expanded in spherical harmonics from $L_{max}=2$ to $L_{max}=18$. Systematically increasing L_{max} has the effect of allowing progressively smaller-scale lateral variations of Vs to affect the vote maps. The Perm Anomaly is clearly defined in all five tomographic models, but only for expansions starting at $L_{max}=12$, indicating its relatively limited spatial extent (<1000 km). Unlike other small-scale features that start to appear at higher-degree expansions but are not present consistently across models, the Perm Anomaly remains remarkably stable as L_{max} increases, further emphasizing the unique character of the Perm Anomaly as a slow feature separated from the two LLSVPs.

We identify the signature of this anomaly directly in waveform data, by looking at shear waves from the deep Spain event of April 11th 2010 (Buforn et al., 2011) that turn near or diffract along the core–mantle boundary (S/Sdiff). A substantial increase in S/Sdiff travel-time delay is observed for paths that traverse the anomaly, compared to nearby paths that do not (Fig. 8c and f). Interestingly, a strong amplitude enhancement is observed in these waveforms (Fig. 8e), suggesting that the velocity gradients associated with the Perm Anomaly effectively focus seismic energy. Observations of delays and amplitude focusing can also be seen at longer periods, which strongly indicates that the anomaly extends hundreds of kilometers above the CMB, and is in contrast to the behavior observed for ultra-low velocity zones (e.g. Cottaar and Romanowicz, in press). The fact that shear waves north of the anomaly do not exhibit travel-time delays implies that the anomaly cannot be connected to the northernmost region of the African LLSVP.

Forward modeling with the coupled spectral element method (Capdeville et al., 2003) demonstrates that a simplified cylindrical shear velocity perturbation of at least -6%, $\sim$900 km in diameter at the CMB, and 370 km in height above the CMB is necessary to produce the observed amplitude enhancements and travel-time delays. This large Vs reduction inferred from waveform modeling suggests that the relatively small size of the Perm Anomaly causes tomographic models to underestimate its strength compared to the LLSVPs. The travel time anomalies observed in the 35°–40° azimuth range suggest a degree of complexity in the northern boundary of the Perm Anomaly that cannot be due to thermal effects alone; the fact that this boundary appears to be irregular in the tomographic models indicates that these are able to capture the fine details of the boundary. Therefore, the Perm Anomaly, like the LLSVPs, appears to have seismically sharp boundaries. However, its Vs reduction is smaller and the height larger, than the 10–30% drops and tens of kilometer height typically found within ULVZs (Garnero and McNamara, 2008).

While wavefront healing effects may hide smaller anomalies (Hwang et al., 2011), the fact that we detect only one anomaly of this kind implies that the process that led to its formation is rare, though not necessarily unique. We do not know what this process is, but a successful dynamic model would have to account for its formation. In particular, it would be informative to investigate how the Perm anomaly ties into models in which the shapes of long-lived thermochemical piles on the CMB are dictated by past subduction history (McNamara and Zhong, 2005), or where LLSVPs represent a non-random agglomeration of "normal size" plumes (Schubert et al., 2004). There does not seem to be a reciprocal process: there is no blue anomaly enclosed in a big red one. The detection of a slow anomaly within a fast region is all the more remarkable because it is made more difficult by wavefront healing effects that render slow anomalies harder to detect; fast anomalies are not masked by a reciprocal effect (Nolet and Dahlen, 2000). Therefore, it is possible that other, smaller "Perm-type" anomalies will be identified by future studies.

Are there other substantial velocity anomalies common to all the models within or outside the LLSVPs that are simply hidden by the dominant long-wavelength structure of the lower mantle? In order to address this possibility, we map the median magnitude of horizontal velocity gradients across the five tomographic models (Fig. 9) and find that large gradients highlight the margins of both LLSVPs as well as the margins of the Perm Anomaly. Because velocity gradients depend on short wavelength structure, this confirms that the Perm Anomaly is unusual both in its absolute Vs – to which the cluster analysis is sensitive – and in

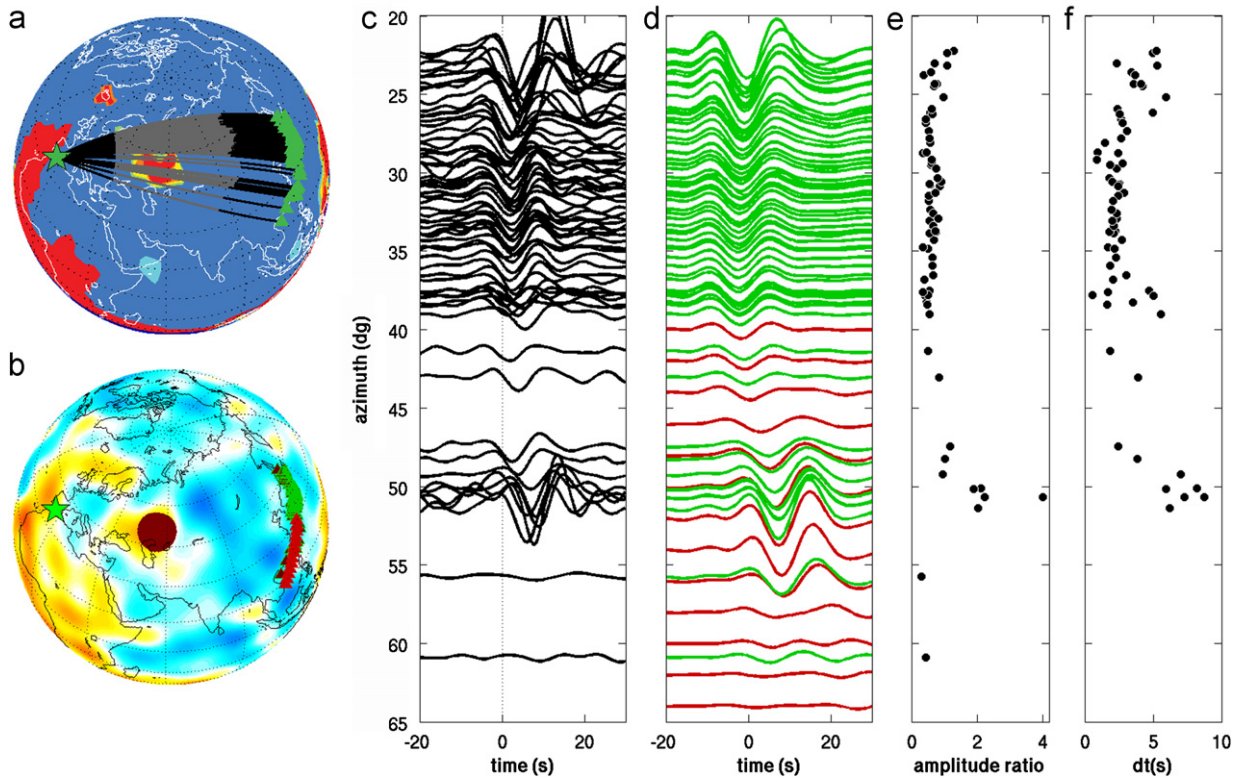

Fig. 8. Seismic transverse-component velocity waveforms from the deep Spain event of April 11th 2010 (Buforn et al. 2011) observed at 66 stations in the 91°–102° distance range show travel time delays and amplitude focusing due to the "Perm Anomaly." (a) Great circle paths and their relation to the Perm anomaly. Lighter shading indicates the portion of the path within the D″ region. Triangles indicate stations. (b) Simple cylindrical 3D model that best reproduces first order features in the data. The model includes a 370 km high cylinder with a diameter of 900 km (at the CMB) and a velocity reduction of −6% centered at 54°E, 50°N. The background model is SAW24B16 (Mégnin and Romanowicz, 2000). Real stations (green) are augmented with a set of hypothetical stations (red) to complement available azimuthal coverage. (c) Observed and (d) synthetic S/Sdiff waveforms filtered between 10–30 s and ordered as a function of azimuth. Strong travel time delays and amplitude focusing due to the Perm anomaly appear around 50° in azimuth. No similar time delays are observed to the north, indicating that the Perm Anomaly is not connected to the Iceland region of the African LLSVP. The same color convention is used for synthetic traces as in (b). Observed Sdiff amplitude ratios (e) and differential travel times (f) as a function of azimuth, referred to 1D normal mode synthetics. Travel time measurements could not be made for the nodal traces at the largest azimuths. (For interpretation of the references to color in this figure legend, the reader is referred to the web version of this article.)

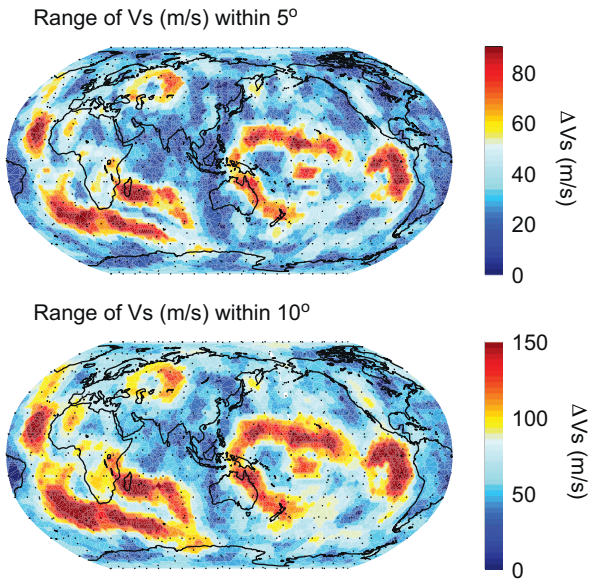

Fig. 9. Margins of both LLSVPs and the Perm Anomaly are characterized by a steep gradient of Vs, here represented by the median range of Vs (m/s) over a distance of 5° and 10° in the five models considered. Away from the margins of the LLSVPs and the Perm Anomaly, lateral velocity gradients are very small, indicating relative uniformity within the LLSVPs and in the ring of faster-than-average velocities.

the magnitude of the horizontal Vs gradients bounding it. Fig. 9 also shows that Vs is relatively laterally uniform within the LLSVPs and the surrounding fast region. The only exception to this intra-LLSVP uniformity is an area of enhanced lateral Vs gradients to the south of Hawai'i (e.g. Russell et al., 1999), which may be associated with smaller-scale structures similar to those detected within the LLSVP to the northwest (Russell et al., 1999; To et al., 2011; Cottaar and Romanowicz, in press).

When might have the Perm Anomaly formed? If the LLSVPs are very ancient, could such a small anomaly exist by itself for very long? If it is a young feature, then the Perm Anomaly may offer a clue as to how LLSVPs are formed. On the other hand, the Perm Anomaly may be quite old: it is intriguing that the location of the anomaly is very close to the restored location (Torsvik et al., 2008) of the eruption of the Siberian Traps that punctuated the end of the Permian period (see Fig. 2). Though far from conclusive, this coincidence may indicate that the Perm Anomaly's diminutive size resulted from substantial flux out of the anomaly.

4. Conclusions

We have performed cluster analysis on lower mantle Vs profiles from 5 recent global tomographic models. For all models, there is a simple separation of lower mantle structure into two slow and one fast region, each of which is geographically

contiguous. In fact, we find that for the vast majority of points on the Earth, all the tomographic models agree on the classification of the associated Vs profiles with either the slow or fast region. The boundaries of these regions are generally collocated across models; the agreement between the boundaries obtained through cluster analysis and locations determined by detailed waveform-modeling studies strongly indicates that tomographic models are reliable on <1000 km scale.

The single exception to this simple separation of lower mantle structure is an isolated, $\sim$900 km wide slow anomaly that we call the "Perm Anomaly"; we cannot rule out the existence of smaller, Perm-type anomalies, which may be more difficult to detect due to wavefront healing effects. The recovery of the Perm Anomaly confirms that the resolution of the data sets used in global tomographic inversions is sufficient to robustly resolve velocity anomalies of this size, regardless of the theory, parameterization and regularization used in inversion. Therefore, models of the lowermost mantle are truly dominated by long wavelength features which are not a consequence of limited resolution of seismic tomography.

Though substantially smaller than LLSVP, the Perm Anomaly has a similar Vs reduction and is bounded by similarly strong Vs lateral gradients as detected along the margins of the LLSVPs. It appears to be different from ULVZs, which have a much smaller vertical extent and greater Vs anomalies. These characteristics are consistent with the interpretation that the Perm Anomaly is made of similar material as the LLSVPs, material which is likely to be compositionally distinct from that in the "fast" cluster.

We find that for all tomographic models, the velocity gradients in the fast and slow regions are asymmetric in the lowermost 500 km of the mantle – a region we dub the "abyssal region." Furthermore, the velocity differences between their profiles span the range of Vs predicted for end-member lower mantle compositions (Matas et al., 2007). These characteristics of Vs structure within the abyssal region highlight the need to take into account the different velocity profiles of slow and fast regions when pursuing mineralogical interpretations. The average velocity profiles characterizing our "slow" and "fast" clusters can serve as reference models for mineralogical interpretations of lower mantle elastic properties in terms of temperature and composition that are likely to be more meaningful than interpretations based on global averages.

Finally, while agreement between models degrades somewhat in the mid-mantle, there is still a clear indication that the slow regions extend into the transition zone, although perhaps somewhat broader and less contiguous in geographical extent.

Acknowledgments

This work was supported by the National Science Foundation Grant nos. EAR0738284 and EAR1067513 and an European Research Council grant WAVETOMO to B.R., EAR-0838304 to A.M.D and an NSF-EAR Postdoctoral Fellowship to V.L. (EAR0948303). We thank C. Houser, B. Kustowski, N. Simmons, and J. Ritsema for making their models available. We thank the editor, Peter M. Shearer, as well as Saskia Goes and an anonymous reviewer for suggestions that markedly improved the manuscript. This is Berkeley Seismological Laboratory contribution 12–14.

References

Andrault, D., Munoz, M., Bolfan-Casanova, N., Guignot, N., Perrillat, J.-P., Aquilanti, G., Pascarelli, S., 2010. Experimental evidence for perovskite and post-perovskite coexistence throughout the whole D″ region. Earth Planet. Sci. Lett. 293, 90–96.

Beibin, L., McDonald, C., 1993. Comparing three classification strategies for use in ecology. J. Veg. Sci. 4 (3), 341–348.

Boschi, L., Dziewonski, A.M., 1999. High- and low-resolution images of the Earth's mantle: implications of different approaches to tomographic modeling. J. Geophys. Res. 104, 25567–25594.

Buforn, E., Pro, C., Cesca, S., Udías, A., del Fresno, C., 2011. The 2010 Grenada, Spain, deep earthquake. Bull. Seism. Soc. Am. 1, 2418–2430, http://dx.doi.org/10.1785/0120110022.

Capdeville, Y., Chaljub, E., Vilotte, J.P., Montagner, J.P., 2003. Coupling the spectral element method with a modal solution for elastic wave propagation in global earth models. Geophys. J. Int. 152 (1), 34–67, http://dx.doi.org/10.1046/j.1365-246X.2003.01808.x.

Clevede, E., Megnin, C., Romanowicz, B., Lognonne, P., 2000. Seismic waveform modeling and surface wave tomography in a three-dimensional Earth: asymptotic and non-asymptotic approaches. Phys. Earth Planet. Inter. 119, 37–56.

Cottaar, S., Romanowicz, B., 2012. An unusually large ULVZ at the base of the mantle beneath Hawaii. Earth Planet. Sci. Lett. http://dx.doi.org/10.1016/j.epsl.2012.09.005.

Dziewonski, A.M., Anderson, D., 1981. Preliminary reference Earth model. Phys. Earth Planet. Inter. 25 (4), 297–356.

Dziewonski, A.M., Lekic, V., Romanowicz, B., 2010. Mantle anchor structure: an argument for bottom up tectonics. Earth Planet. Sci. Lett. 299, 69–79.

Evritt, B.S., Gourlay, A.J., Kendell, R.E., 1971. An attempt at validation of traditional psychiatric syndromes by cluster analysis. Br. J. Psychiatry 119, 399–412.

Filsinger, E.E., Faulkner, J.E., Warland, R.H., 1979. Empirical taxonomy of religious individuals: an investigation among college students. Sociol. Relig. 40 (2), 136–146.

Garnero, E.J., McNamara, A.K., 2008. Structure and dynamics of Earth's lower mantle. Science 320 (5876), 626–628, http://dx.doi.org/10.1126/science.1148028.

Grocholski, B., Catalli, K., Shim, S.-H., Prakapenka, V., 2012. Mineralogical effects on the detectability of the postperovskite boundary. Proc. Nat. Acad. Sci. 109 (7), 2275–2279.

Harris, N.M., Gurnell, A.M., Hannah, D.M.P.G.E., 2000. Classification of river regimes: a context for hydroecology. Hydrol. Process. 14, 2831–2848.

Hernlund, J.W., Houser, C., 2008. On the distribution of seismic velocities in Earth's deep mantle. Earth Planet. Sci. Lett. 265, 423–437.

He, Y., Wen, L., 2009. Structural features and shear-velocity structure of the "Pacific Anomaly". J. Geophys. Res. 114 (B02309), http://dx.doi.org/10.1029/2008JB005814.

He, Y., Wen, L., Zheng, T., 2006. Geographic boundary and shear wave velocity structure of the "Pacific anomaly" near the core–mantle boundary beneath western Pacific. Earth Planet. Sci. Lett. 244, 302–314.

Houser, C., Masters, G., Shearer, P., Laske, G., 2008. Shear and compressional velocity models of the mantle from cluster analysis of long-period waveforms. Geophys. J. Int. 174, 195–212, http://dx.doi.org/10.1111/j.1365-246X.2008.03763.x.

Hwang, Y.K., Ritsema, J., van Keken, P.E., Goes, S., Styles, E., 2011. Wavefront healing renders deep plumes seismically invisible. Geophys. J. Int. 187 (1), 273–277, http://dx.doi.org/10.1111/j.1365-246X.2011.05173.x.

Iitaka, T., Hirose, K., Kawamura, K., Murakami, M., 2004. The elasticity of the $MgSiO_3$ post-perovskite phase in the Earth's lowermost mantle. Nature 430, 442–445.

Jordan, T., Puster, P., Glatzmaier, G., Tackley, P., 1993. Comparisons between seismic Earth structures and mantle flow models based on radial correlation functions. Science 261 (5127), 1427–1431.

Kellogg, L.H., Hager, B.H., van der Hilst, R., 1999. Compositional stratification in the deep mantle. Science 283 (5409), 1881–1884, http://dx.doi.org/10.1126/science.283.5409.1881.

Kennett, B.N.L., Engdahl, R., Buland, R., 1995. Constraints on seismic velocities in the Earth from travel times. Geophys. J. Int. 122, 108–124.

Kustowski, B., Ekstrom, G., Dziewonski, A.M., 2008. Anisotropic shear-wave velocity structure of the Earth's mantle: a global model. J. Geophys. Res. 113, (B06306). http://dx.doi.org/10.1029/2007JB005169.

Lekic, V., Romanowicz, B., 2011. Tectonic regionalization without a priori information: a cluster analysis of upper mantle tomography. Earth Planet. Sci. Lett. 308 (1–2), 151–160, http://dx.doi.org/10.1016/j.epsl.2011.05.050.

Li, X.-D., Romanowicz, B., 1995. Comparison of global waveform inversions with and without considering cross-branch modal coupling. Geophys. J. Int. 121, 695–709.

Luhr, J.F., Navarro-Ochoa, C., Savov, I.P., 2010. Tephrochronology, petrology and geochemistry of late-Holocene pyroclastic deposits from Volcan de Colima, Mexico. J. Volcanol. Geotherm. Res 197, 1–32.

MacQueen, J., 1967. Some methods for classification and analysis of multivariate observations. In: Proceedings of the Fifth Berkeley Symposium on Mathematical Statistics and Probability, vol. 1. pp. 281–297.

Manners, U., 2008. Investigating the core–mantle boundary region with S and P diffracted waves. Ph.D. Thesis. University of California, San Diego.

Masters, G., Laske, G., Bolton, H., Dziewonski, A.M., 2000. The relative behavior of shear velocity, bulk sound speed, and compressional velocity in the mantle: implications for chemical and thermal structure. In: Karato, S., Forte, A.M., Liebermann, R.C., Masters, G., Stixrude, L. (Eds.), Earth's deep interior: mineral physics and omography from the atomic to the global scale. American Geophysical Union, Washington, DC.

Matas, J., Bass, J., Ricard, Y., Mattern, E., Bukowinski, M.S.T., 2007. On the bulk composition of the lower mantle: predictions and limitations from generalized inversion of radial seismic profiles. Geophys. J. Int. 170, 764–780, http://dx.doi.org/10.1111/j.1365-246X.2007.03454.x.

Matas, J., Bukowinski, M.S.T., 2007. On the anelastic contribution to the temperature dependence of lower mantle seismic velocities. Earth Planet. Sci. Lett. 259, 51–65.

McNamara, A.K., Garnero, E.J., Rost, S., 2010. Tracking deep mantle reservoirs with ultra-low velocity zones. Earth Planet. Sci. Lett. 299, 1–9, http://dx.doi.org/10.1016/j.epsl.2010.07.042.

McNamara, A.K., Zhong, S., 2005. Thermochemical structures beneath Africa and the Pacific Ocean. Nature 437, 1136–1139, http://dx.doi.org/10.1038/nature04066.

Megnin, C., Romanowicz, B., 1999. The effects of the theoretical formalism and data selection on mantle models derived from waveform tomography. Geophy. J. Int. 138, 366–380.

Mégnin, C., Romanowicz, B., 2000. The three-dimensional shear velocity structure of the mantle from the inversion of body, surface and higher-mode waveforms. Geophys. J. Int. 143 (3), 709–728, http://dx.doi.org/10.1046/j.1365-246X.2000.00298.x.

Montelli, R., Nolet, G., Fahlen, F.A., Masters, G., Engdahl, E.R.H.S.-H., 2004. Finite-frequency tomography reveals a variety of plumes in the mantle. Science 303, 338–343.

Mosca, I., Cobden, L., Deuss, A., Ritsema, J., Trampert, J., 2012. Seismic and mineralogical structures of the lower mantle from probabilistic tomography. J. Geophys. Res. 117 (B06304), http://dx.doi.org/10.1029/2011JB00851.

Murakami, M., Hirose, K., Kawamure, K., Sata, N., Ishishi, Y., 2004. Post-perovskite phase transition in $MgSiO_3$. Science 304, 855–857.

Ni, S., Helmberger, D.V., Tromp, J., 2005. Three-dimensional structure of the African superplume from waveform modelling. Geophys. J. Int. 161, 283–294.

Ni, S., Tan, E., Gurnis, M., Helmberger, D.V., 2002a. Sharp sides to the African superplume. Science 296, 1850–1852.

Ni, D., Tan, E., Gurnis, M., Helmberger, D., 2002b. Sharp sides to the African Superplume. Science 296 (5574), 1850–1852.

Nolet, G., Dahlen, F.A., 2000. Wave front healing and the evolution of seismic delay times. J. Geophys. Res. 105, 19043–19054.

Oganov, A.R., Ono, S., 2004. Theoretical and experimental evidence for a post-perovskite phase of $MgSiO_3$ in Earth's D″ layer. Nature 430, 445–448.

Ohta, K., Hirose, K., Lay, T., Sata, N., Ohishi, Y., 2008. Phase transitions in pyrolite and MORB at lowermost mantle conditions: implications for a MORB-rich pile above the core–mantle boundary. Earth Planet. Sci. Lett. 267, 107–117.

Punj, G., Stewart, D.W., 1983. Cluster analysis in marketing research: review and suggestions for application. J. Market. Res. 20, 134–148.

Ritsema, J., Deuss, A., van Heijst, H.J., Woodhouse, J.H., 2011. S40RTS: a degree-40 shear-velocity model for the mantle from new Rayleigh wave dispersion, teleseismic traveltime and normal-mode splitting function measurements. Geophys. J. Int. 184, 1223–1236, http://dx.doi.org/10.1111/j.1365-246X.2010.04884.x.

Ritsema, J., Ni, S., Helmberger, D.V., Crotwell, H.P., 1998. Evidence for strong shear velocity reductions and velocity gradients in he lower mantle beneath Africa. Geophys. Res. Lett. 25 (23), 4245–4258.

Robertson, S.G., Woodhouse, J.W., 1996. Ratio of relative S to P velocity heterogeneity in the lower mantle. J. Geophys. Res. 101, 20041–20052.

Romanowicz, B., Gung, Y.-C., 2002. Superplumes from the core–mantle boundary to the lithosphere: implications for heat flux. Science 296 (5567), 513–516.

Russell, S.A., Lay, T., Garnero, E., 1999. Small-scale lateral shear velocity and anisotropy heterogeneity near the core–mantle boundary beneath the central Pacific imaged using broadband ScS waves. J. Geophys. Res. 104 (B6), 13183–13199.

Schubert, G., Masters, G., Olson, P., Tackley, P., 2004. Superplumes or plume clusters? Phys. Earth Planet. Inter. 146, 147–162.

Simmons, N.A., Forte, A., Boschi, L., Grand, S., 2010. GyPSuM: a joint tomographic model of mantle density and seismic wave speeds. J. Geophys. Res. 115 (B12310), http://dx.doi.org/10.1029/2010JB007631.

Spetzler, J., Trampert, J., 2003. Implementing spectral leakage corrections in global surface wave tomography. Geophys. J. Int. 155 (2), 532–538.

Steinberger, B., 2000. Plumes in a convecting mantle: models and observations for individual hotspots. J. Geophys. Res. 105 (B5), 11127–11152.

Su, W.J., Dziewonski, A.M., 1997. Simultaneous inversion for 3-D variations in shear and bulk velocity in the mantle. Phys. Earth Planet. Inter. 100, 135–156.

Takeuchi, N., Morita, Y., Xuyen, N.D., Zung, N.Q., 2008. Extent of the low-velocity region in the lowermost mantle beneath the western Pacific detected by the Vietnamese broadband seismograph array. Geophys. Res. Lett. 35 (L05307), http://dx.doi.org/10.1029/2008GL033197.

Thorne, M.S., Garnero, E.J., 2004. Inferences on ultralow-velocity zone structure from global analysis of SPdKS waves. J. Geophys. Res. 109 (B08301), http://dx.doi.org/10.1029/2004JB003010.

To, A., Capdeville, Y., Romanowicz, B, 2005. 3D effects of sharp boundaries at the borders of the African and Pacific superplumes: observation and modeling. Earth Planet. Sci. Lett. 233, 137–153, http://dx.doi.org/10.1016/j.epsl.2005.01.037.

To, A., Fukao, Y., Tsuboi, S, 2011. Evidence for a thick and localized ultra low shear velocity zone at the base of the mantle beneath the central Pacific. Phys. Earth Planet. Inter. 184, 119–133.

Torsvik, T.H., Steinberger, B., Cocks, L.R.M., Burke, K., 2008. Longitude: linking Earth's ancient surface to its deep interior. Earth Planet. Sci. Lett. 276, 273–282, http://dx.doi.org/10.1016/j.epsl.2008.09.026.

Trampert, J., Deschamps, F., Resovsky, J., Yuen, D., 2004. Probabilistic tomography maps chemical heterogeneities throughout the lower mantle. Science 306 (5697), 853–856, http://dx.doi.org/10.1126/science.1101996.

Trampert, J., Snieder, R., 1996. Model estimations biased by truncated expansions: possible artifacts in seismic tomography. Science 271 (5253), 1257–1260.

Trampert, J., Spetzler, J., 2006. Surface wave tomography: finite-frequency effects lost in the null space. Geophys. J. Int. 164, 394–400.

Tsuchiya, T., Tsuchiya, J., Unemoto, K., Wentzcovitch, 2004. Elasticity of post-perovskite $MgSiO_3$. Geophys. Res. Lett. 31 (L14603), http://dx.doi.org/10.1029/2004GL020278.

Wang, Z., Dahlen, F.A., 1995. Sphericalspline parameterization of threedimensional earth models. Geophys. Res. Lett. 22 (22), 3099–3102, http://dx.doi.org/10.1029/95GL03080.

Wen, L., 2001a. Seismic evidence for a rapidly varying compositional anomaly. Earth Planet. Sci. Lett. 194, 83–95.

Wen, L., 2001b. Seismic evidence for a rapidly varying compositional anomaly at the base of the Earth's mantle beneath the Indian Ocean. Earth Planet. Sci. Lett 194, 83–95.

Wen, L., Silver, P., James, D., Kuehnel, R., 2001. Seismic evidence for a thermo-chemical boundary at the base of the Earth's mantle. Earth Planet. Sci. Lett. 189, 141–153.

Woodhouse, J.H., Dziewonski, A.M., 1984. Mapping the upper mantle: three-dimensional modeling of earth structure by inversion of seismic waveforms. J. Geophys. Res. 89 (B7), 5953–5986, http://dx.doi.org/10.1029/JB089iB07p05953.

Wookey, J., Stackhouse, S., Kendall, J.-M., Brodholt, J., Price, G.D., 2005. Efficacy of the post-perovskite phase as an explanation for lowermost-mantle seismic properties. Nature 438, 1004–1007.